Article

Repairing Performance of Polymer-Modified Cement-Based Thin Spray-On Liners on Pre-Cracked Rock-like Specimens

Jinlong Teng [1], Xiaotong Yu [1], Ping Wang [2], Guoming Liu [1,*], Lingnan Cui [1] and Xiangfei Cui [1]

1 College of Safety and Environmental Engineering, Shandong University of Science and Technology, Qingdao 266590, China; tjlnzx4373@163.com (J.T.); 15166250603@163.com (X.Y.); skcln502@163.com (L.C.); skd994394@sdust.edu.cn (X.C.)
2 Zaozhuang Mining Group Xin'an Coal Industry Co., Zaozhuang 277642, China; wpxamk@163.com
* Correspondence: lgmrenqing@163.com or skd995978@sdust.edu.cn

Abstract: With the development of coal mining and the increase in excavation depth, the stress on roadway surrounding rock is also increasing. This creates conditions for crack development in the roadway, so it is urgent to develop rock repair materials with excellent performance. The ability of thin spray-on liner (TSL) to repair rock and concrete opens up the possibility of reusing abandoned roadways. The ability of TSL to support the surrounding rock is also important in preventing the generation of roadway waste. In this paper, styrene–acrylic emulsion (SAE), vinyl acetate–ethylene copolymer emulsion (VAE), and polyvinyl alcohol powder (PVA) were used to prepare three TSLs. Rock-like materials were configured using cement mortar according to similar principles. Three types of TSLs were tested for basic properties such as viscosity and mechanical strength, which provided data to support the explanation of the repair performance of TSLs. Three TSLs were used to repair pre-cracked rock-like specimens (PR). The number of brushing times and the angle of PR's cracks were regarded as test variables. Changes in the mechanical strength of repaired PRs were tested by compressive and flexural tests. TSL repair performance was evaluated with the help of mechanical strength changes. Results show that polyvinyl alcohol powder modified cement-based thin spray-on liner is most suitable for repairing rock cracks; as the thickness of the brush slurry increases, its repair performance continues to improve. This paper can provide experience and a theoretical basis for the research of other rock repair materials, and it is also instructive for repairing shotcrete in the roadway.

Keywords: thin spray-on liners; compressive strength; flexural strength; repair; polymer

1. Introduction

Thin spray-on liner (TSL) is a new rock repair and support technology that is widely used in coal mining for roadway support and surrounding rock repair engineering. It is expected that this technology will replace traditional support systems (anchor mesh support and shotcrete). The performance of TSL is between shotcrete and wire mesh. Compared with shotcrete, TSL has the advantages of a short maintenance cycle, fast application, high tensile strength, good bonding performance, prevention of rock mass loosening, significant ability to penetrate joints, cleanliness, and easy transportation in rock reinforcement [1–9]. Compared with traditional rock support methods, TSL can penetrate into large cracks of the surrounding rock with its excellent flowability, and gradually fill the capillary cracks of the surrounding rock. TSL can bond both sides of the cracks and bond the failed rock body into a complete composite structure, thereby producing a repair effect on the surrounding rock. When the composite structure receives external loads, TSL, as a bonding intermediate of the rock mass, can also withstand some of these loads. This puts forward the requirements for basic mechanical properties of TSL, such as compressive and flexural resistance. [10–12].

Tannant [13] has pointed out that the performance characteristics of TSL are between shotcrete and anchor network support. TSL is a supplement to these types of support and

is receiving more and more attention. However, most scholars have focused on the support properties of TSL, and less research has been done on the rock-repairing ability of TSL.

TSL is defined as a new coating material with excellent mechanical properties. TSL covers the surrounding rock of the roadway with a very thin (<10 mm) chemical coating, thus providing support, sealing, and barrier effects. TSL is generally divided into three main categories, namely, cement-based TSL, polymer-based TSL, and latex-based TSL. TSL consists of two main components: a liquid–liquid mixture or a liquid–powder mixture, which need to be mixed immediately prior to application, then mixed well and immediately sprayed onto the rock surface. TSL penetrates rock cracks with the help of its own fluidity, fills the cracks, and binds the sides of the cracks, thus repairing the rock.

One of the key parameters affecting the repair ability of TSL is its bonding ability with the sprayed rock surface. This bonding ability can prevent the loosening of the rock and stop the further development of cracks. Li et al. [14] investigated and quantified the effects of rock strength and surface roughness on the bond strength of TSL layers through experimental tests. They found a bilinear relationship between bond strength and matrix strength, and they also found that the bond strength of TSL increased significantly with the increase in surface roughness of the sprayed rock surface. Yilmaz et al. [15] studied the bond strength of various TSLs with different curing times, and the results showed that most TSL bond strengths were proportional to the curing time. Ozturk et al. [16] tested the adhesion strength of TSL on different substrate materials, and they found that the bond strength of TSL on sandstone, granite, and common surrounding rock was 11.4 MPa, 0.4 MPa, and 3.7 MPa, which is higher than the bond strength of concrete materials to each substrate material in shotcrete technology. Qiao et al. [17] conducted uniaxial compression experiments using TSL coated on the surfaces of different types of rocks (siltstone, sandstone, granite). TSL support was more significant for weaker rocks. Ozturk et al. [18,19] quantitatively investigated the effect of TSL material thickness on its adhesion force, and the results showed that the adhesion force was inversely proportional to the square root of thickness.

The above literature has studied the effects of substrate surface roughness, substrate strength, substrate material, TSL material curing time, and TSL material thickness on bond strength. However, there has been limited study on the rock repair ability exhibited by TSL bonding performance. The mechanism of the effect of polymer addition on TSL repair performance is not clear. Few tests have directly studied the change in strength of damaged rock after TSL injection.

Most of the TSLs commonly used in the present are cement-based and polymer-based, and the input cost of cement-based TSLs is lower compared to polymer-based TSLs. Therefore, cement-based TSLs modified with polymers were chosen for this experiment.

Several formulations of TSL have been published in the literature [19–21], and this paper is a continuation of these studies. In this study, VAE, SAE, and PVA were selected as modified polymers, and some additional fillers and admixtures were added to configure a fixed dose of TSL. In this experiment, three kinds of TSLs were prepared based on the above materials, namely, vinyl acetate–ethylene copolymer emulsion-modified cement-based thin spray-on liner (VTSL), styrene–acrylic emulsion-modified cement-based thin spray-on liner (STSL), and polyvinyl alcohol powder modified cement-based thin spray-on liner (PTSL). The flowability, viscosity, and basic mechanical properties of TSL were tested and combined with previous studies to analyze the repair mechanism of TSL. Since natural rock cracks are difficult to form regularly, in this paper, rock-like materials were prepared using cement mortar based on similar principles. A new method was used to pre-fabricate rock cracks with three angles (0°, 45°, 90°). Brushing thickness was also a variable in this paper, and the effect of different brushing thicknesses on the effectiveness of TSL repair was investigated. The experiment tested the compressive and flexural strength of pre-cracked rock-like specimens repaired by polymer-modified cement-based thin spray-on liners (PR-TSL), and the variation of their compressive and flexural strength characterized the repair performance of TSL.

In short, this paper investigates the repair ability of polymer-modified cement-based TSL, which can provide experience and theoretical basis for the research of other rock repair materials and provide new ideas for the repair and prevention of rock cracks. Since the rock-like material is made from cement mortar, the study of the repair capability of TSL is also instructive for repairing shotcrete in the roadway. This is of great significance in preventing the development of cracks in the surrounding rock and promoting safe production. The repair of cracks can also further enhance the support capacity of rock and shotcrete, and improve the service life of tunnels and buildings, which has a certain economic value.

2. Materials and Experiments

In this paper, three TSLs were prepared. The raw materials used to prepare them were polymers, cement, and various admixtures. It is worth noting that the polymers used to prepare the three TSLs are different. Rock-like materials were prepared using cement mortar based on the formulation provided by previous studies. This material was used to prepare rock-like specimens. After that, three types of cracks were prepared in rock-like specimens using self-designed method; PR was obtained. The extensibility, viscosity, compressive strength, and flexural strength of the three TSLs were tested. The compressive strength and flexural strength of the PR-TSL were tested.

2.1. Raw Materials

In this experiment, three TSLs were prepared based on cement and modified by polymer. Since natural rock cracks are difficult to form regularly, rock-like materials were used to prepare the rocks required for the test. A new method was designed to prepare regular cracks at three angles (0°, 45°, 90°).

1.   Cement

The cement used is P·O 42.5 ordinary silicate cement, which conforms to the standard ASTM C150 (Standard Specification for Portland Cement) with a specific surface area of 338 m^2/kg. Table 1 shows the main chemical composition of the cement.

Table 1. The main chemical composition of cement.

Component	SiO$_2$	Al$_2$O$_3$	Fe$_2$O$_3$	CaO	MgO	SO$_3$
Content (wt%)	20.81	4.54	3.15	64.22	2	2.5

2.   Fillers

Light calcium carbonate: it is a white solid powder with no irritating odor. Particle size is about 5 μm. It is slightly hygroscopic, stable in dry air, decomposed in acid, and produced by Qingdao Urso Chemical Technology Co. (Qingdao, China). It is used in this experiment for TSL.

Natural river sand: it is mainly diffuse sedimentary sand, with off-white-gray-yellow color. The fineness modulus is 2.80, water content is 2.3%, mud content is 2.4%, and the apparent density is 2600 kg/m³. Figure 1 shows the set curve of river sand, complying with the Chinese standard GB 50086-2015 (Technical Specification for Geotechnical Anchor and Shotcrete Support Works). Figure 1 shows in detail the grain size distribution of river sand. It is used in this experiment to prepare PR.
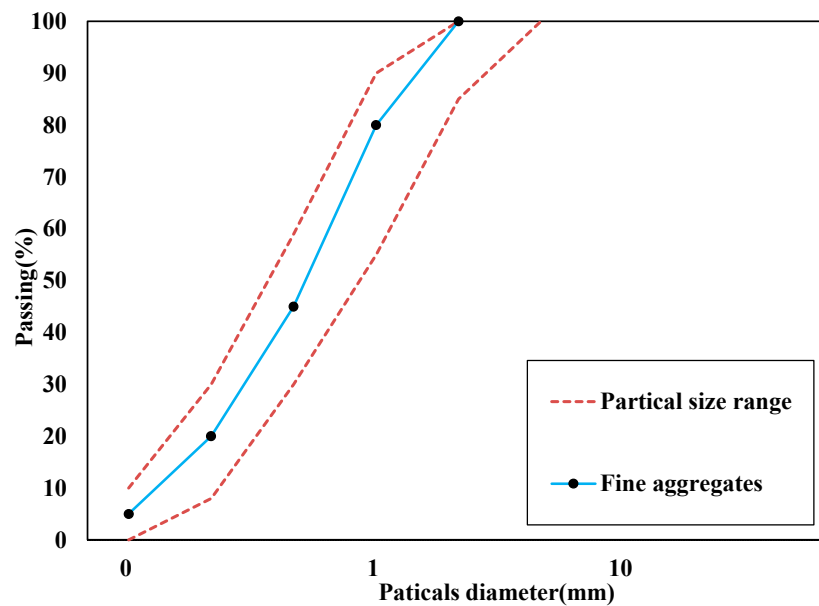
Figure 1. Sand assembly curve.

3.   Admixtures

Cement accelerator: it is a brownish powder that can play a role in accelerating the effect of hydration and hardening of TSL, and its water content is less than 2%, which complies with the standard of GB 50119-2016 (Concrete admixture application technical specifications). Polycarboxylic acid water reducer: it is a white powder that can improve the workability of cement slurry, reduce the water consumption in the cement mixing process, and improve the fluidity of the slurry. Its water content is less than or equal to 3.0%, and it complies with the GB 50119-2016 (Concrete admixture application technical specifications). Dodecyl alcohol ester film-forming agent: it is a white transparent liquid that can effectively reduce the film-forming temperature of the polymer. Polydimethylsiloxane defoamer: this is a milky white liquid that can effectively eliminate the air bubbles generated by mixing the polymer with water; therefore, it can reduce the porosity of the slurry and thus enhance the internal compactness of the material, and it has a solid content of 10%. Cellulose: it is a white powder with no irritating odor and no toxicity, which can play a role in water retention.

4.   Vinyl acetate–ethylene copolymer emulsion (VAE)

It consists of vinyl acetate and ethylene monomer, its color is milky white, and the phase is liquid, as shown in Figure 2. The specific technical specifications of the VAE used in the test are shown in Table 2, produced by Qingdao Urso Chemical Technology Co. (Qingdao, China).


Figure 2. VAE.

Table 2. Technical specifications of VAE.

Particle Size (μm)	Solid Content (%)	Viscosity (MPa·s)	pH	Minimum Film Forming Temperature (°C)	Dilution Stability (%)
2	54.5	500–1000	4.0–6.0	0	3.5

5.   Styrene propylene emulsion (SAE)

It is obtained by emulsion copolymerization of styrene and acrylate monomer, with a cream color, light blue luster, and liquid phase, as shown in Figure 3. It has good physical and chemical properties, high temperature resistance, and good anti-aging properties. It has a solid content of 40%, viscosity of 80–3000 MPa·s, pH of 8–9, a minimum film-forming temperature of 22 °C, and it is produced by Qingdao Urso Chemical Technology Co. (Qingdao, China).
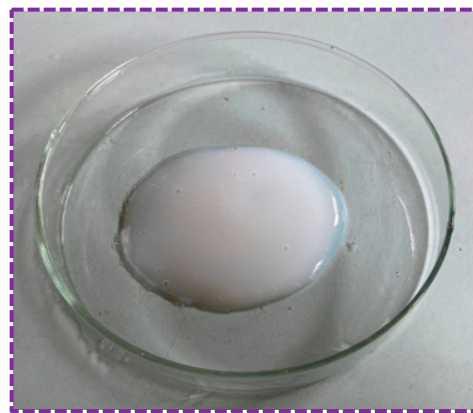
Figure 3. SAE.

6.   Polyvinyl alcohol powder (PVA)

The powder is usually polymerized with vinyl acetate as the monomer, which is then alcoholized or hydrolyzed to make polyvinyl alcohol. It is a white, non-toxic, and odorless powder solid, as shown in Figure 4. The aqueous solution's pH of polyvinyl alcohol powder is 4.5–6.5. It has a minimum film-forming temperature of 2 °C and is produced by Qingdao Urso Chemical Technology Co. (Qingdao, China).


Figure 4. PVA.

2.2. Ratio of TSL

In this experiment, VAE, SAE, and PVA were selected to modify the cement-based TSL, and three TSLs were obtained, namely VTSL, STSL, and PTSL. This experiment was

a continuation of the existing research, and the following ratios were obtained from the existing literature [19–21]. The water–cement ratio (W/C) was set to 50%. The poly–cement ratio (P/C) was set to 10%. The ratio of light calcium carbonate to cement mass (L/C) was set to 5%. The ratio of cellulose to cement mass (Ce/C) was set to 0.4. The ratio of accelerator to cement mass (A/C) was set to 4%. The ratio of water reducer to cement mass (R/C) was set to 0.5%. The ratio of defoamer to polymer mass (D/P) was set to 0.2%. The ratio of film-forming agent to polymer mass (F/P) was set to 1%. The detailed proportions of the raw materials are listed in Table 3. It should be noted that for polymeric materials where the phase is a polymer emulsion, the mass of the polymer is obtained by multiplying the mass of the emulsion with its solid ratio. The remaining mass is considered to be the mass of water. So, the mass of water obtained by calculating the water–ash ratio includes the mass of water in the emulsion and the mass of water alone. Figure 5 shows the three TSL repair materials prepared. As can be seen in Figure 5, the STSL surface was guilty of a light blue color, the VTSL was light gray, and the PTSL appeared to have a higher viscosity.

Table 3. Specific ratio of TSL.

W/C	P/C	L/C	Ce/C	A/C	R/C	D/P	F/P
50%	10%	5%	0.4%	4%	0.5%	0.2%	1%
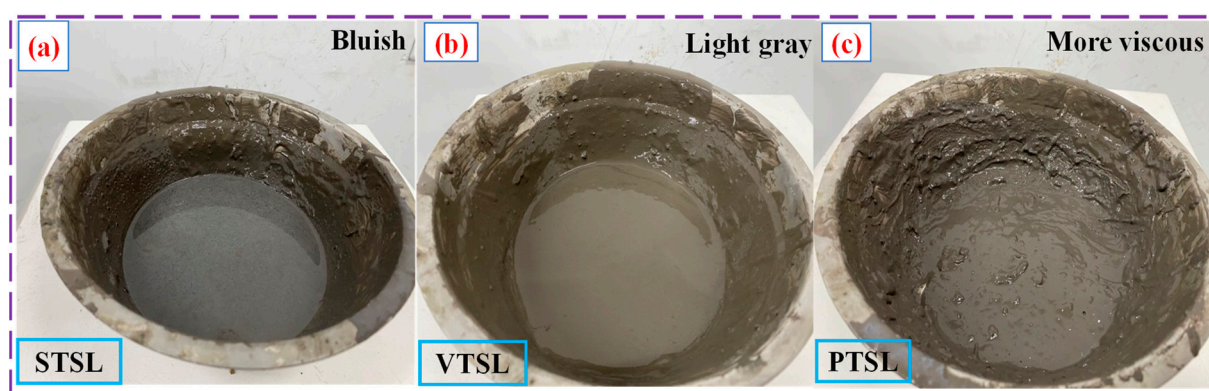
Figure 5. Three types of TSL. (**a**): STSL; (**b**): VTSL; (**c**): PTSL.

2.3. Preparation and Grouping of PR

In this experiment, ordinary cement mortar was used as the rock-like material to make rock-like specimens. The ratio of rock-like material was determined as cement, fine sand, and water mass ratio = $M_{cement}:M_{sand}:M_{water} = 5:5:2$, according to the literature and similar theorems [22–24].

The preparation of PR was carried out strictly according to Chinese standards GB/T 17671-1999 (Cementitious sand strength test method) and DL/T5126-2001 (Polymer modified cement mortar test procedure), and the molds used were 40 mm × 40 mm × 160 mm triplex molds.

The specific operation steps were: (1) cement, fine sand, and water were mixed well beforehand, then loaded into the triclinic mold and densely vibrated on a vibrating table. (2) The specimens were first cured under natural conditions for 4 h, and three angles of the cracks were prepared on the specimens. The plastic tube was pressed in the center of the specimens with a certain strength until the plastic tube was completely in the specimens, after which the plastic tube was carefully removed. The diameter of the plastic tube was 4 mm and the length was 20 mm, as shown in Figure 6b. The prefabricated crack was 4 mm deep, 4 mm wide, and 20 mm long, and it was tilted at 0°, 45° and 90°, as shown in Figure 6c. (3) After that, the specimens continued to be set in the triclinic mold for 20 h and then demolded. (4) The demolded specimens were cured in water for 7 d and then cured

for 28 d in nature. The curing temperature fluctuated between 23 °C and 26 °C. The whole preparation process is shown in Figure 6.
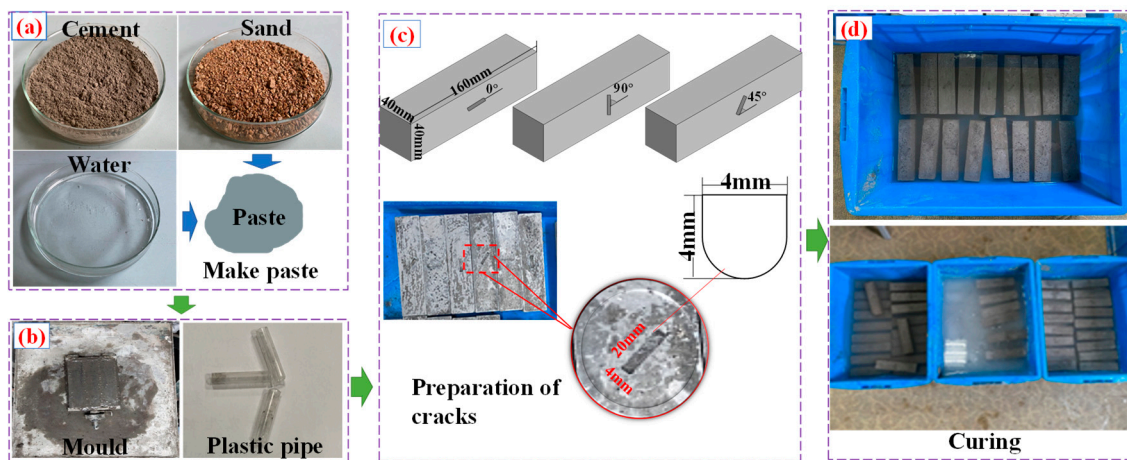
Figure 6. Preparation of PR. (**a**): Raw materials for preparation of rock-like materials; (**b**): triplex mold and plastic tubes; (**c**): preparation of cracks; (**d**): curing of specimens.

According to the type of polymer, the angle of prefabricated cracks, and the number of times TSL was brushed, the following grouping can be obtained, as seen in Table 4. In Table 4, odd-numbered specimens would be used for the compressive test, and even-numbered specimens would be used for the flexural test. "C" represents the control group, where specimens in the C-1 and C-2 groups are not treated in any way. However, both group C-3 and group C-4 need to prepare three kinds of cracks at 0°, 45° and 90°. "STSL, VTSL, PTSL" refers to the TSL applied by each group, and the number of brushing times for each group has been detailed in Table 4. It should be added that the groups starting with "STSL, VTSL, PTSL" need to prepare cracks at 0°, 45° and 90°. According to the requirements of Table 4, TSL was brushed on PR, and PR-TSL were obtained, after which compressive and flexural tests were conducted.

Table 4. Test grouping for repair of PR.

Group	Crack Angle (Angle with Pressure Direction)	Brushing Times	Test Type
C-1	-	-	Compression test
C-2	-	-	Flexural test
C-3	0°, 45°, 90°	-	Compression test
C-4	0°, 45°, 90°	-	Flexural test
STSL-5	0°, 45°, 90°	1	Compression test
STSL-6	0°, 45°, 90°	1	Flexural test
STSL-7	0°, 45°, 90°	2	Compression test
STSL-8	0°, 45°, 90°	2	Flexural test
STSL-9	0°, 45°, 90°	3	Compression test
STSL-10	0°, 45°, 90°	3	Flexural test
VTSL-11	0°, 45°, 90°	1	Compression test
VTSL-12	0°, 45°, 90°	1	Flexural test
VTSL-13	0°, 45°, 90°	2	Compression test
VTSL-14	0°, 45°, 90°	2	Flexural test
VTSL-15	0°, 45°, 90°	3	Compression test
VTSL-16	0°, 45°, 90°	3	Flexural test
PTSL-17	0°, 45°, 90°	1	Compression test

Table 4. *Cont.*

Group	Crack Angle (Angle with Pressure Direction)	Brushing Times	Test Type
PTSL-18	0°, 45°, 90°	1	Flexural test
PTSL-19	0°, 45°, 90°	2	Compression test
PTSL-20	0°, 45°, 90°	2	Flexural test
PTSL-21	0°, 45°, 90°	3	Compression test
PTSL-22	0°, 45°, 90°	3	Flexural test

2.4. Test Methods

In this experiment, the fluidity, viscosity, and basic mechanical properties of three TSLs were tested at first. Testing TSLs' fluidity can help us understand the mechanism of TSL crack penetration. Testing the viscosity and mechanical strength of TSLs were important to analyze the repair mechanisms of TSLs. Thus, TSL basic performance tests provided data to support tests of TSL repair performance. Then, TSL repair tests were conducted. TSLs were painted around the cracks of rock-like specimens, and after curing for 7 d, changes in compressive and flexural strength of PR-TSL were compared to characterize the repair effect of TSLs.

(1)   TSL basic performance tests

The flow extensibility, viscosity, and compressive and flexural strength of three TSLs were tested. The flow extensibility of freshly mixed TSL was measured using a Cone mold conforming to GB/T 8077-2012 (Concrete admixture homogeneity test method); the viscosity of TSL was measured using NDJ-79 rotary viscometer produced by Shanghai Precision Instruments & Meters Co (Shanghai, China). The steps of the extensibility test and viscosity test are shown in Figure 7. Compressive and flexural tests were conducted according to GB/T 17671-1999 (Cementitious sand strength test method).


Figure 7. Extensibility test and viscosity test. (**a**): Raw materials for TSL preparation; (**b**): preparation of TSL slurry; (**c**): extensibility text; (**d**): viscosity test.

(2)   Repair tests of TSL

The repair performance of TSL was tested according to a self-designed test method. TSLs were pre-prepared and brushed on PR, according to Table 4. TSLs were applied around the cracks of rock-like specimens with a brush. The range of the brushed TSL was about 30 mm above and below the center of the crack's midpoint. The thickness of the brushed TSL was characterized by the number of brushing times. The thickness of brushed TSL represented by different brushing times was measured. The thickness of brushed TSL

was approximately 1.5 mm for one brushing, 2.8 mm for two brushings, and 4.2 mm for three brushings.

After that, PR-TSL were placed under natural conditions for 7 d, and the curing temperature fluctuated between 23 °C and 26 °C. Chen et al. [19] found in their study that the bond strength was basically unchanged when the TSL curing time was greater than 7 d. Therefore, in this experiment, we decided to cure PR-TSL under natural conditions for 7 d. After the repair was completed, PR-TSL needed to be tested for compressive and flexural strength, and the whole experimental procedure is shown in Figure 8. The compressive and flexural tests were carried out according to GB/T 17671-1999 (Cementitious sand strength test method). Figure 9 shows the schematic diagram of the compressive test, flexural test, and the damage of the PR-TSL.
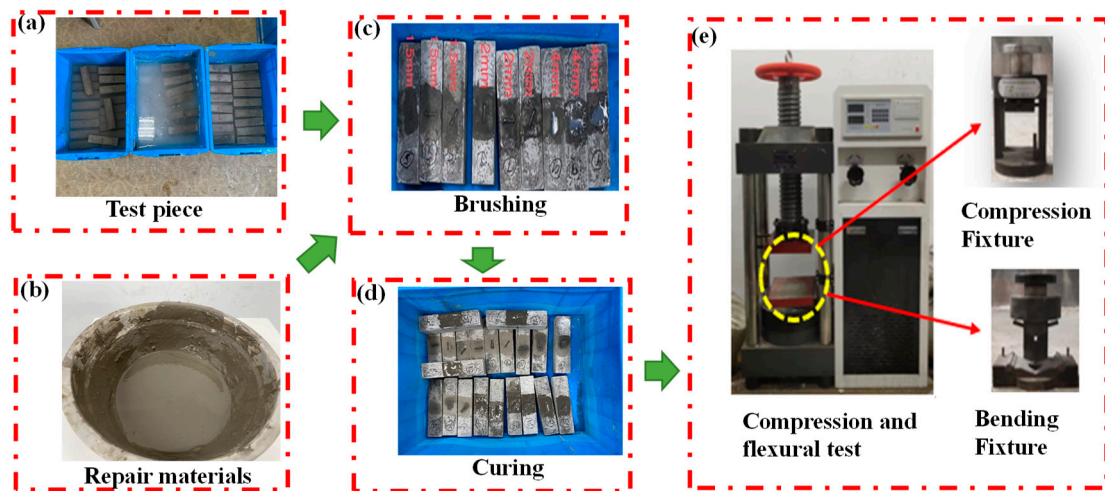
Figure 8. TSL repair test steps. (**a**): Cured test specimens; (**b**): preparation of TSL; (**c**): brushed TSL for repair; (**d**): PR-TSL curing; (**e**): repair tests of TSL.
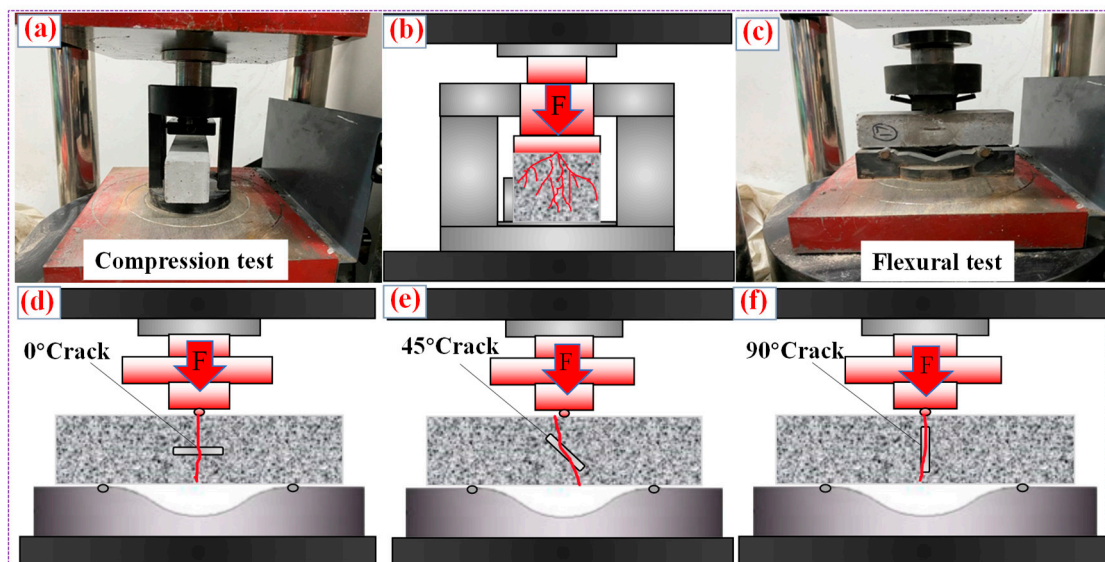
Figure 9. Schematic diagram of the compressive test, flexural test, and the damage of the PR-TSL. (**a**): Compression test; (**b**): schematic diagram of the test specimen being damaged by pressure; (**c**): flexural test; (**d**): schematic diagram of the 0° test specimen being damaged by bending; (**e**): schematic diagram of the 45° test specimen being damaged by bending; (**f**): schematic diagram of the 90° test specimen being damaged by bending.

3. Results and Discussion

In the process of cement-based TSL repair, a series of physicochemical reactions will occur, and the amount of brushing TSL will produce different repair effects on different cracks. A large amount of domestic and foreign literature has shown that in roadway engineering, many types of cracks are produced on the surface of or inside the rock. The development process of these cracks is different, so these rocks exhibit different mechanical properties. Moreover, the compressive and flexural strength of cementitious materials do not improve after the addition of polymer admixture into cement; they may even show a decreasing trend. Of course, there is information suggesting that polymer admixture can significantly improve the compressive and flexural strength of cementitious materials [25–30].

3.1. Basic Performance of TSL

The basic properties of the three TSLs measured in the test are shown in Table 5. The ratio of flexural strength to compressive strength responds to the toughness of the TSL. The larger this ratio, the better the toughness of TSL. The smaller the ratio, the worse the toughness of TSL.

Table 5. Basic performance of TSL.

	Extensibility/ mm	Viscosity/MPa·s	Compressive Strength/MPa	Flexural Strength/MPa	Ratio of Bending to Compression	Air Permeability/cm^3·m^{-2}
STSL	226	1400	16.02	12.89	0.81	1.20×10^6
VTSL	196	3800	19.43	8.98	0.46	1.11×10^6
PTSL	172	4200	22.05	13.47	0.61	1.14×10^6

The test results of the control groups C-1 and C-2 showed that the compressive strength and flexural strength of the rock-like materials were 43.81 MPa and 10.11 MPa, respectively, and the ratio of bending to compression was 0.3. It was evident that the ratio of bending to compression of TSL was significantly higher than that of the rock-like materials, indicating that the toughness of TSL was better. In this experiment, the curing temperature was between 23–26 °C, which was greater than the minimum film-forming temperature of the three polymers. According to the Ohama model [31] and the B-O-V model [32], it is known that the continuous hydration of the cement in TSL glues the polymer particles into a film, forming a spatial mesh structure that enhances the toughness of TSL [33–35], as shown in Figure 10.
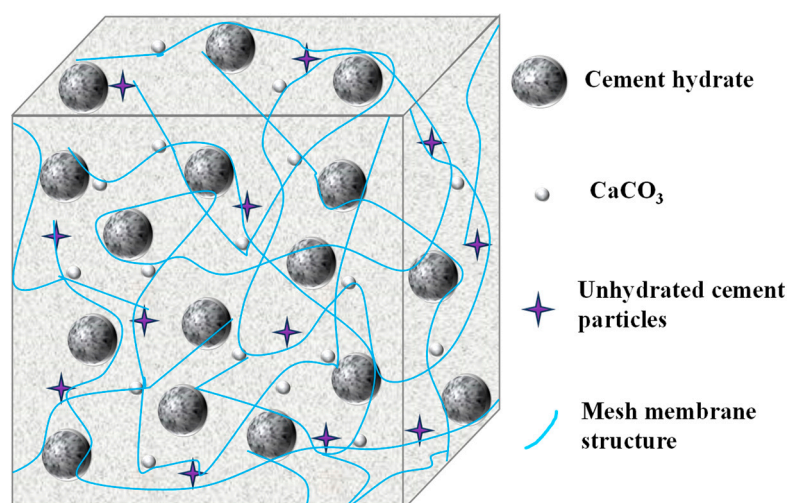

Figure 10. Distribution of polymeric membrane structures in TSL.

3.2. Compressive and Flexural Performance of PR-TSL

Figures 11, 17 and 23 show the changes in compressive strength of PR-TSL. Figures 12, 18 and 24 show the rates of improvement in compressive strength of PR-TSL. Figures 13, 19 and 25 show the changes in flexural strength of PR-TSL. Figures 14, 20 and 26 show the rates of improvement in flexural strength of PR-TSL.

Figures 11–14 indicate the repair effect of STSL on rock-like specimens. From the information in Figures 11 and 13, the R^2 of all six fitted curves is greater than 0.87, which indicates a good fit. Therefore, the repair effect of STSL is consistent with the variation of the relation $y = ax^2 + bx + c$. Both Figures 11 and 13 present the same repair trend of STSL. When the specimen is brushed once, the strength of the specimen shows a decreasing trend. After two brushings, the strength of the specimen is improved compared with that of the specimen brushed once but still lower than that of the specimen without brushing. When the specimen is brushed three times, the strength of the specimen is improved again and can be equal to or even exceed the compressive strength of the specimen without brushing. As shown in Figures 11–14, the repair effect of STSL on rock-like specimens is not obvious enough when the number of brushing times is small, and the rock-like specimens also show a decrease in strength. For 0° specimens, the repair effect is shown when the thickness of brushing slurry is greater than that of point a. For 45° specimens, the repair effect is shown when the thickness of brushing slurry is greater than that of point b. For 90° specimens, the repair effect is shown when the thickness of brushing slurry is greater than that of point c.
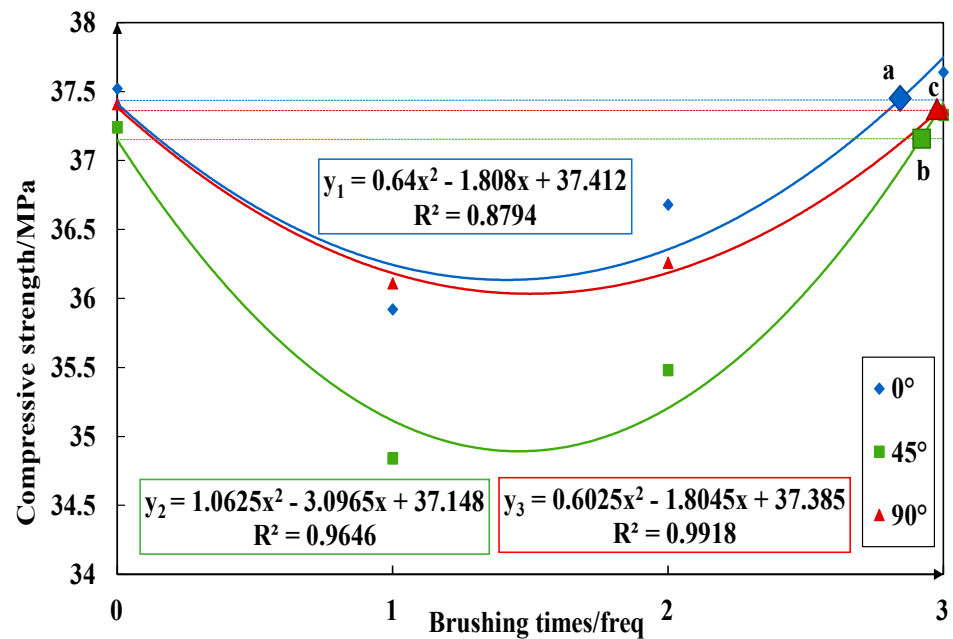

Figure 11. Changes in compressive strength of specimens after repair by STSL.
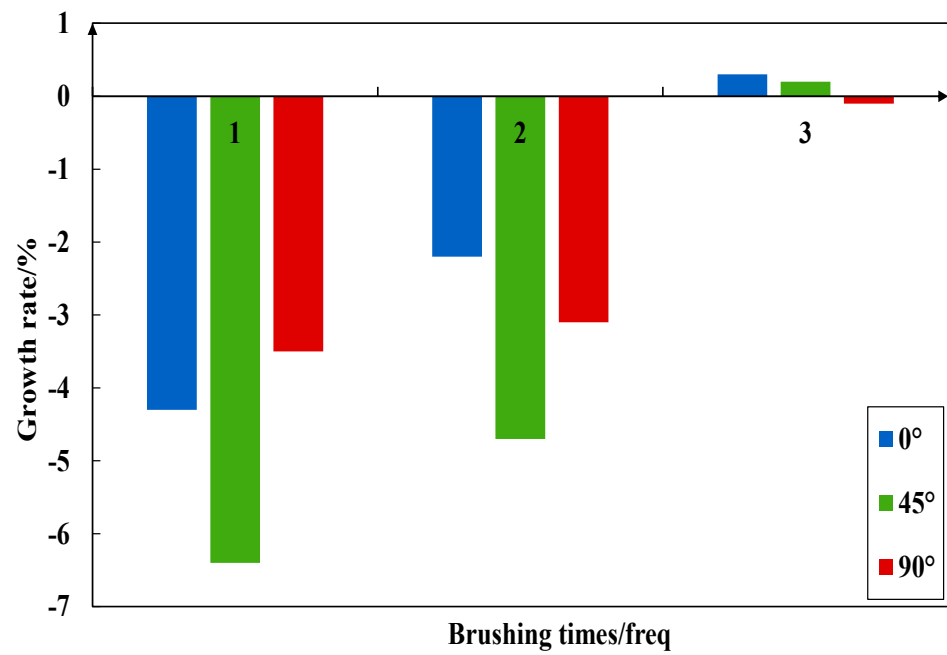
Figure 12. Rate of increase in compressive strength of specimens repaired by STSL.
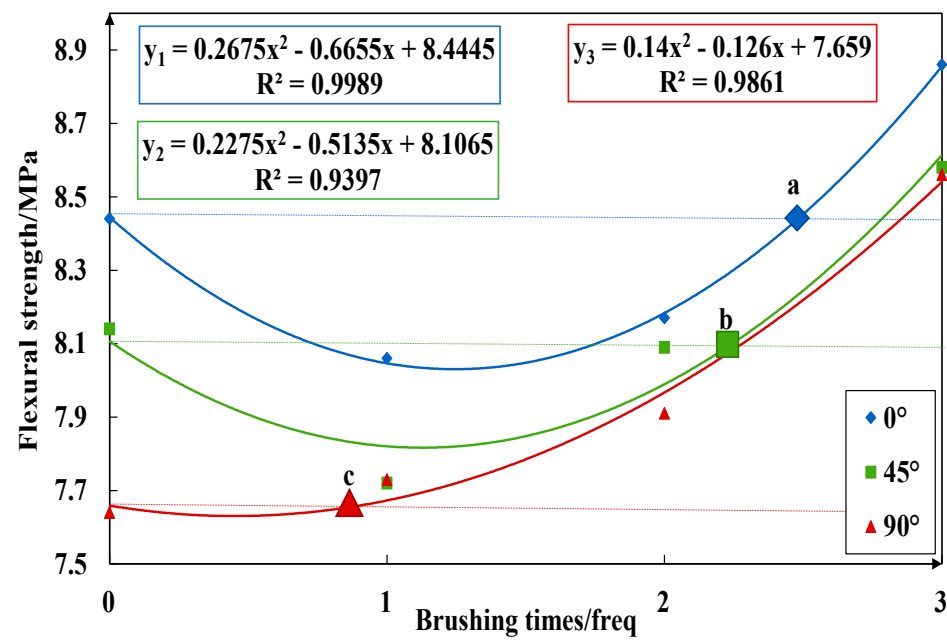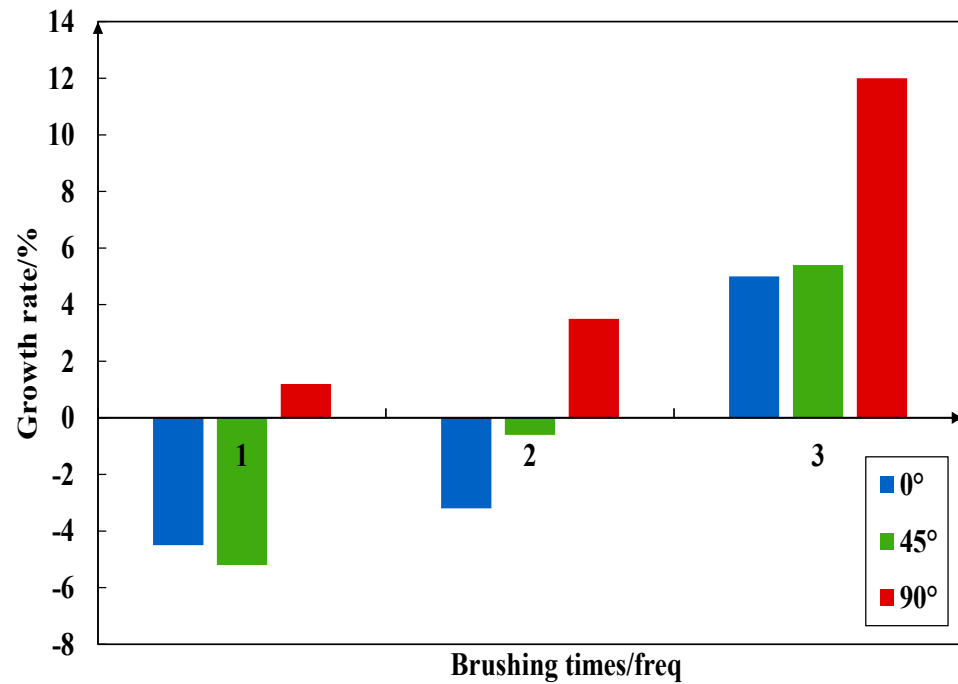

Figure 13. Changes in flexural strength of specimens after repair by STSL.

**Figure 14.** Rate of increase in flexural strength of specimens repaired by STSL.

According to our analysis, STSL has good fluidity and low viscosity. When the number of brushing times is 1 and 2, the thickness of brushing slurry is about 1.5–2.8 mm, and TSL does not occupy the whole crack. The main role in this phase is played by the stress concentration around the crack under external pressure. Moreover, STSL penetrates into the tiny surface cracks and capillaries of PR with its own excellent fluidity. The capillary pore is a hydrophilic capillary pore. Although it is beneficial to the infiltration of STSL, its cement wall surface also absorbs part of the water. This phenomenon is not beneficial to twater participation in the hydration of STSL, so STSL did not reach the expected strength within 7 d. As a result, STSL was brushed around the cracks, an operation similar to adding foreign material into the cracks and capillaries, leading to stress concentrations under pressure [36–38], as shown in Figure 15. The red arrows in Figures 15, 16 and 21 represent stresses. This resulted in damage forming first from around the crack, which is not beneficial to the repair of PR by STSL.
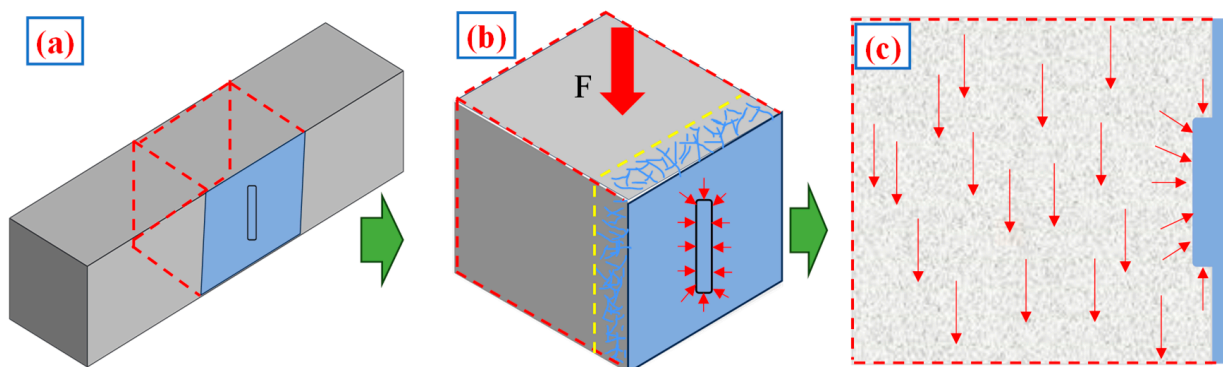
Figure 15. Stress concentration phenomenon at cracks. (**a**): TSL-affected areas, (**b**): invaded cracks, (**c**): concentration of stress.

When the number of brush times was 3, the thickness of brush slurry was about 4.2 mm, which completely occupied the crack surface. At this time, the hydration of STSL played a major role, leading to polymer film formation. With the help of gravity and

capillary effects, STSL easily penetrated into the capillary pores and surface cracks on the surface of the PR. The water molecules were smaller compared with cement particles and polymer particles, so it was easier to move within the cracks. Although capillary pores and crack walls of the PR absorbed part of the water, the amount of absorption was relatively small compared to the whole brushing volume. This had less effect on the hydration of STSL. Within the capillary pores of PR, as the hydration reaction of STSL proceeded, water levels decreased continuously, and the polymer particles agglomerated to form a continuous layer on the surface of unhydrated cement particles, the C-S-H gel, and between aggregates and the polymer cement paste. The intermolecular forces caused the polymer particles to agglomerate into a continuous film, which, together with hydration products, formed a penetrating mesh structure, as shown in Figure 16 [31–35]. STSL can penetrate into the capillary pores and surface cracks of the PR during the repair process. When the capillary holes and surface cracks are compressed, STSL provides good support. When they were tensile, STSL connected the two ends. Thus, it was difficult for the capillary pores and cracks to reach the displacement required for damage, so the repair effect was realized.
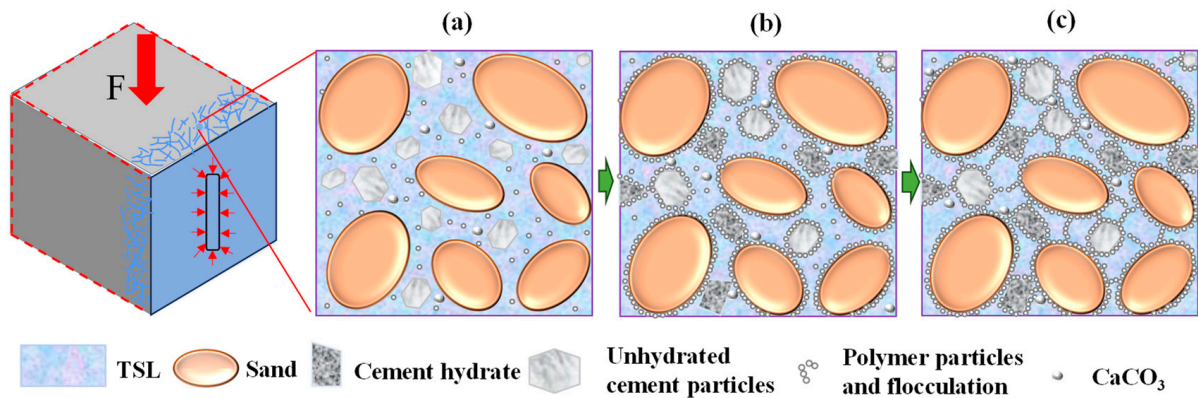
Figure 16. Polymer film formation in the capillaries of rock-like specimens. (**a**): Distribution of TSL in capillaries, (**b**): water decreases as hydration proceeds, (**c**): polymer membrane structure formation.

Figures 17–20 show the effect of VTSL on the repair of PR. From the information in Figures 17 and 19, the R^2 of all six fitted curves is greater than 0.90, which indicates a good fit. Therefore, the repair effect of STSL is in accordance with the variation of the relation $y = ax^2 + bx + c$. The repair trend of VTSL on PR, as indicated in Figure 17, is different from that indicated in Figure 19. The repair trend of VTSL on the compressive strength of specimens decreases and then increases, while the repair trend on flexural strength continuously increases. As shown in Figures 17 and 18, the repair effect of STSL on PR is not obvious enough when the number of brushing times is small, PR-TSL even shows a drop in strength. For 0° specimens, the repair effect is shown when the thickness of brushing slurry is greater than that of point a. For 45° specimens, the repair effect is shown when the thickness of brushing slurry is greater than that of point b. For 90° specimens, the repair effect is shown when the thickness of brushing slurry is greater than that of point c.
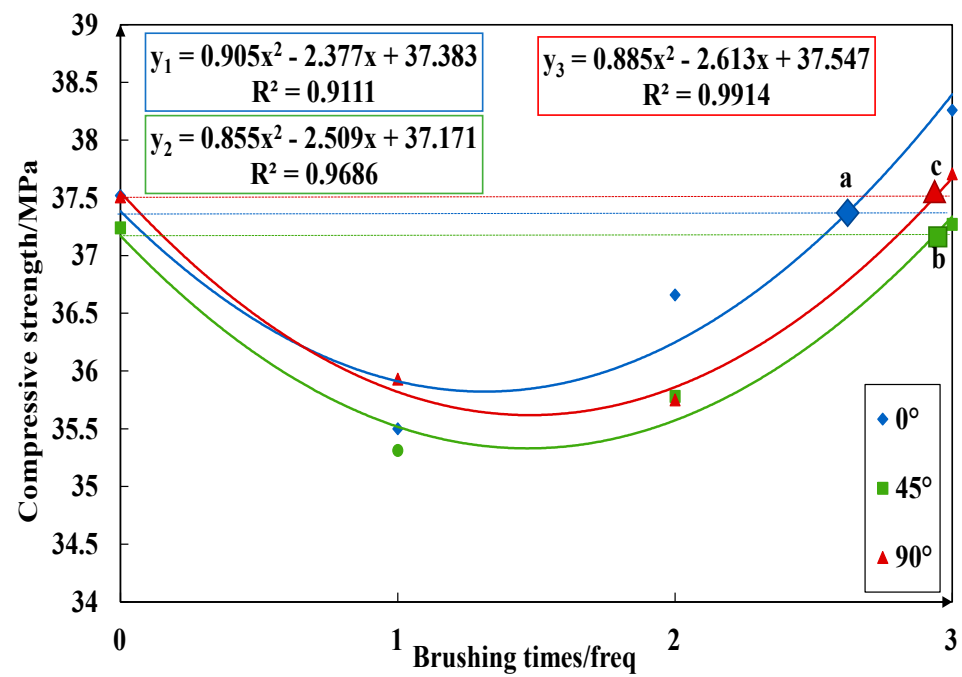
The figure contains the following equations:

$$y_1 = 0.905x^2 - 2.377x + 37.383$$
$$R^2 = 0.9111$$

$$y_2 = 0.855x^2 - 2.509x + 37.171$$
$$R^2 = 0.9686$$

$$y_3 = 0.885x^2 - 2.613x + 37.547$$
$$R^2 = 0.9914$$

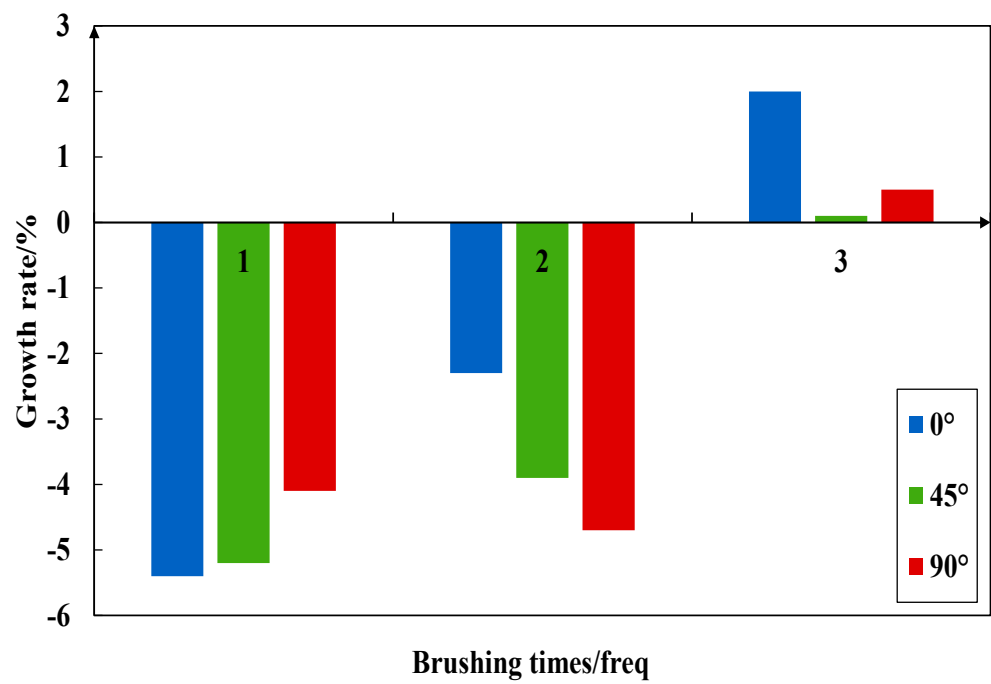**Figure 17.** Changes in compressive strength of specimens after repair by VTSL.

Figure 18. Rate of increase in compressive strength of specimens repaired by VTSL.
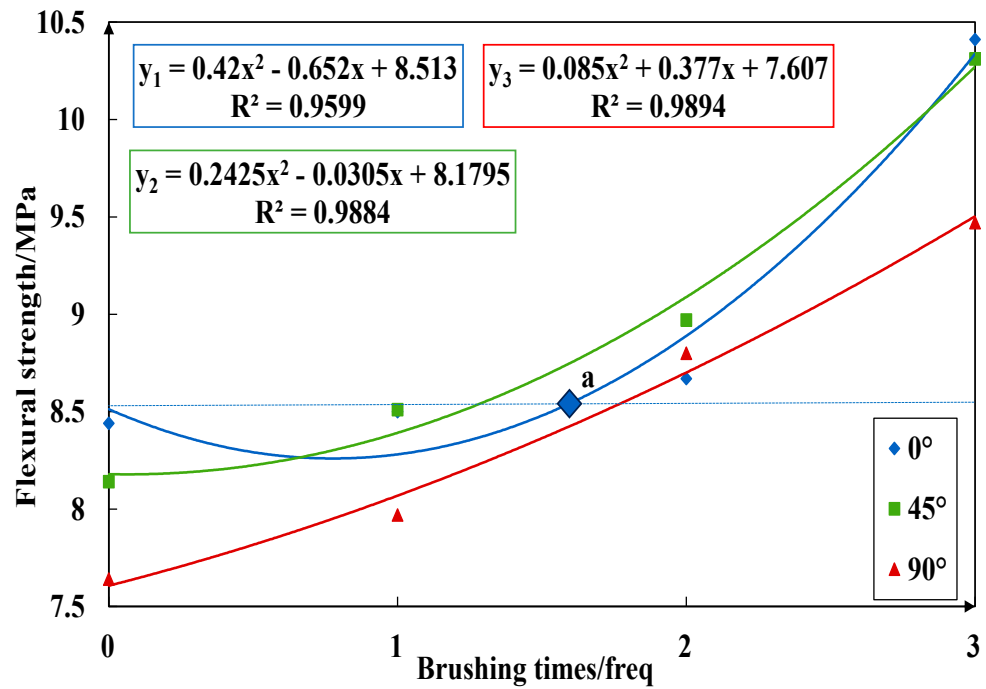
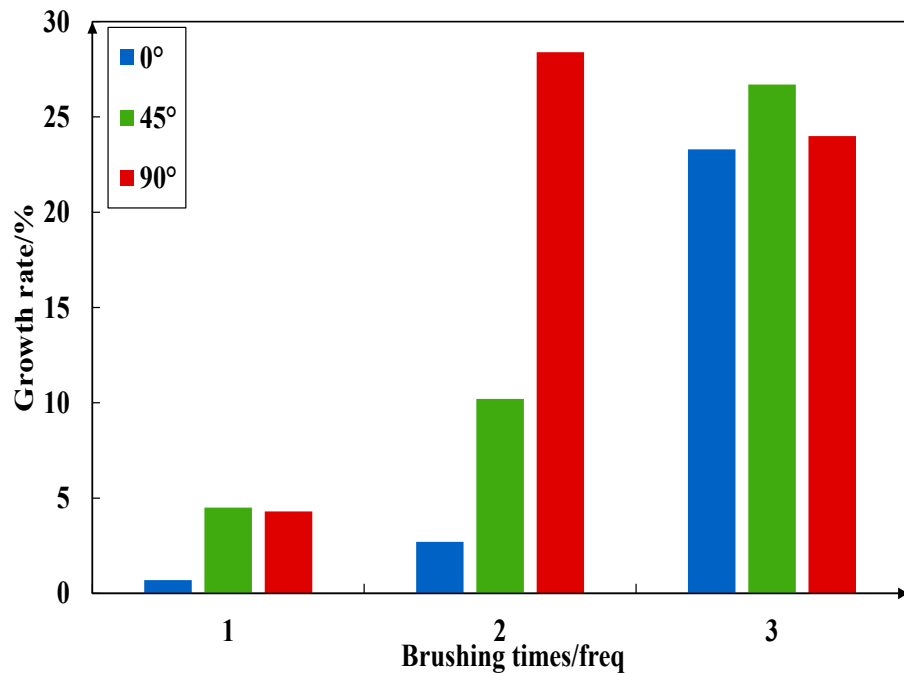**Figure 19.** Changes in flexural strength of specimens after repair by VTSL.

$y_1 = 0.42x^2 - 0.652x + 8.513$
$R^2 = 0.9599$

$y_3 = 0.085x^2 + 0.377x + 7.607$
$R^2 = 0.9894$

$y_2 = 0.2425x^2 - 0.0305x + 8.1795$
$R^2 = 0.9884$

Figure 20. Rate of increase in flexural strength of specimens repaired by VTSL.

According to our analysis, the repair of PR compressive strength by VTSL tended to decrease and then increase. VTSL itself has relatively good fluidity. When applied with 1 or 2 brushings, resulting in a 1.5–2.8 mm thickness of brush slurry, VTSL does not occupy all of the crack. What plays a major role at this phase is the concentration of stresses around the crack under external pressure. The repair effect exhibited at a brush slurry number of 3 can also be explained by the polymer film formation phenomenon. Compared with STSL, the damage effect of VTSL was weaker and the repair effect was stronger, which may be due to the fact that VTSL was less fluid than STSL. The stress concentration area formed by VTSL was smaller than that of STSL, as shown in Figure 21, where the stress concentration

area was within the yellow dashed line. Moreover, the compressive strength of VTSL was 19.43 MPa greater than that of STSL, which was 16.02 MPa. This made VTSL relatively stronger in supporting capillaries and cracks.
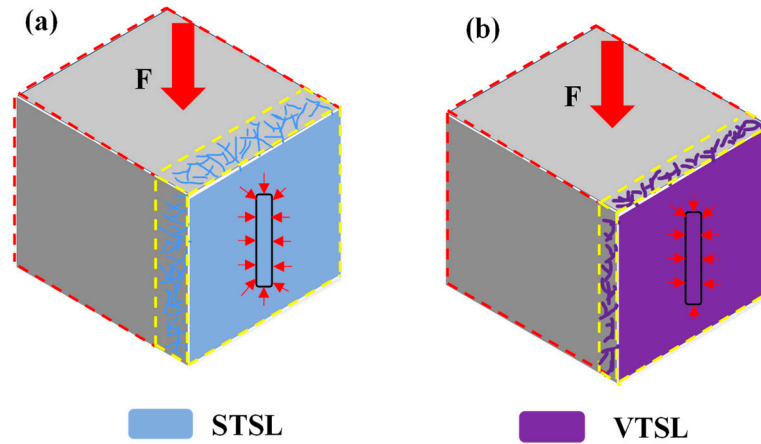
Figure 21. Comparison of STSL and VTSL stress concentration areas. (**a**): Stress concentration area after STSL repair, (**b**): stress concentration area after VTSL repair.

According to our analysis, the repair of PR flexural strength by VTSL tended to increase. The viscosity of VTSL is 3800 MPa·s, which can effectively connect the two ends of the prefabricated cracks and also effectively bond the pore wall in the capillary pore. In the flexural strength test, the area around the crack was mainly affected by the tensile stress. With the help of its high viscosity, VTSL made the connected cracks more resistant to deformation under the influence of external loads. This is due to the polymer membrane structure formed in the VTSL connecting the hydration products of the cement. At the same time, this membrane structure also had a certain tensile strength and bonding strength to hydration products, which made the VTSL less susceptible to deformation, as shown in Figure 22. As the number of brushing times increased, the coverage of the prefabricated cracks and the filling of surface capillaries were higher. The contact area of the TSL with the PR increased, its bond area increased, and the flexural strength of PR continued to increase. Thus, the repair effect of VTSL continued to increase.
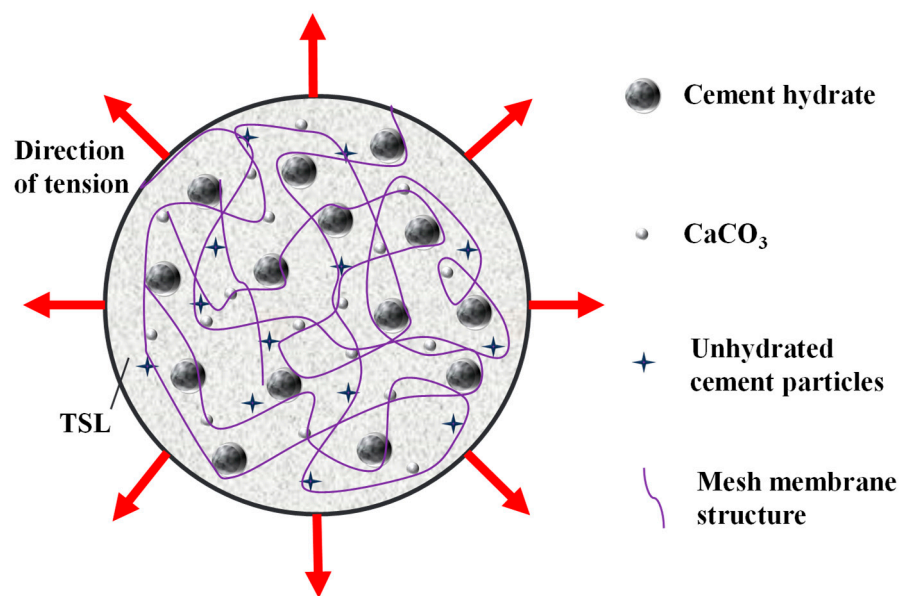
Figure 22. Dispersion diagram of tensile forces on VTSL-bonded cracks and capillaries.

Figures 23–26 imply the effect of PTSL on the repair of PR. From the information in Figures 23 and 25, the R^2 of all six fitted curves is greater than 0.87, which indicates a good fit. Therefore, the repair effect of STSL is in accordance with the variation of the relation $y = ax^2 + bx + c$. The repair trends shown in Figures 23 and 25 show continuous improvement. According to the characteristics of the quadratic equation, the slope of the six trend lines in the figure is the highest when the number of brushing times is 0–1, which indicates that the strength of PR-TSL is improved the most when brushed once. PTSL can achieve a good repair effect, but the repair effect is not improved significantly with the increase in brushing times.

$$y_1 = 0.115x^2 + 1.233x + 37.678$$
$$R^2 = 0.9616$$

$$y_2 = -0.2025x^2 + 2.3145x + 36.914$$
$$R^2 = 0.8743$$

$$y_3 = -0.3225x^2 + 1.9665x + 37.456$$
$$R^2 = 0.9921$$
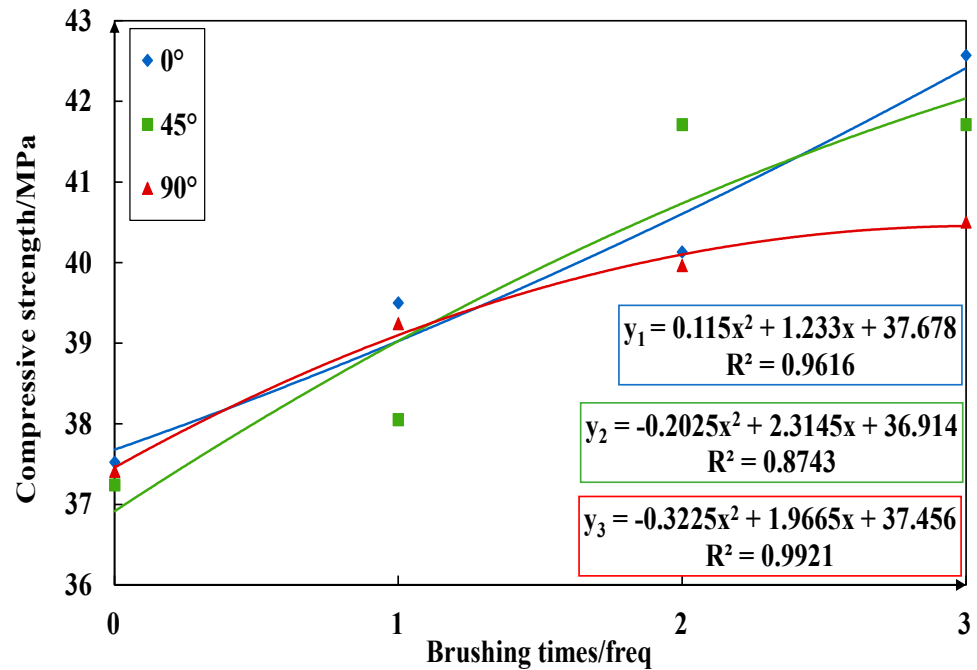
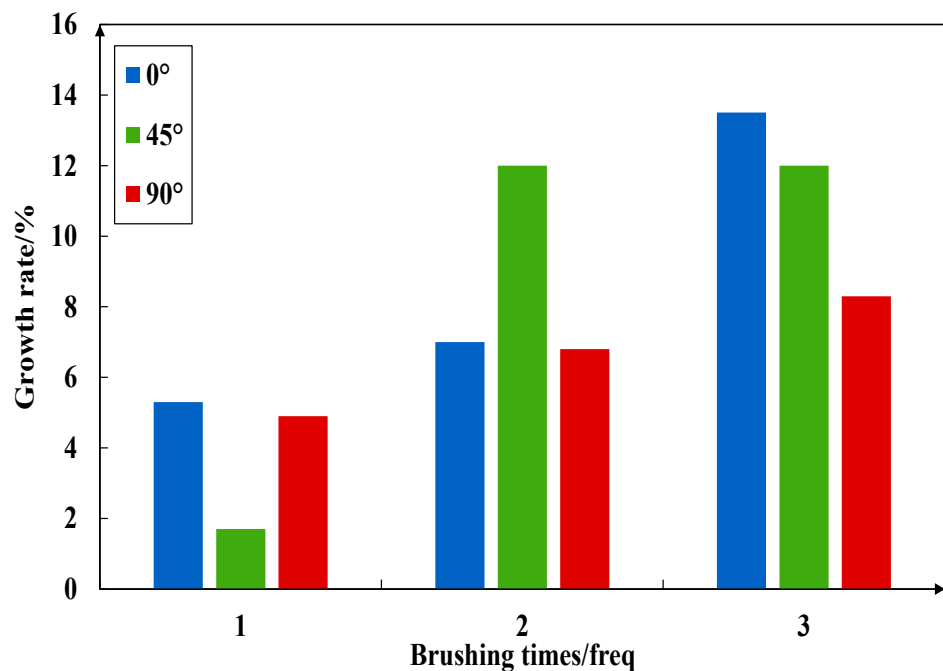**Figure 23.** Changes in compressive strength of specimens after repair by PTSL.

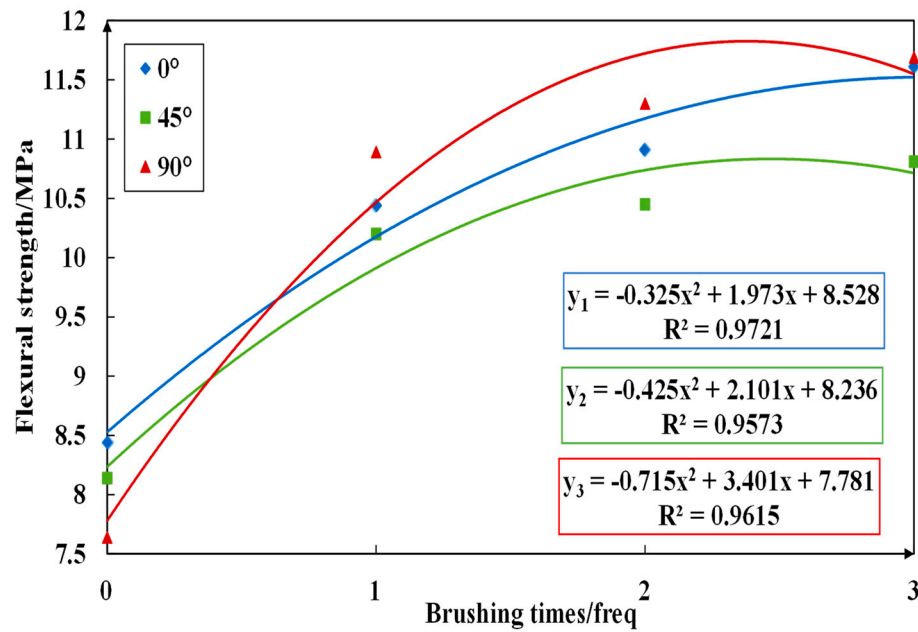**Figure 24.** Rate of increase in compressive strength of specimens repaired by PTSL.

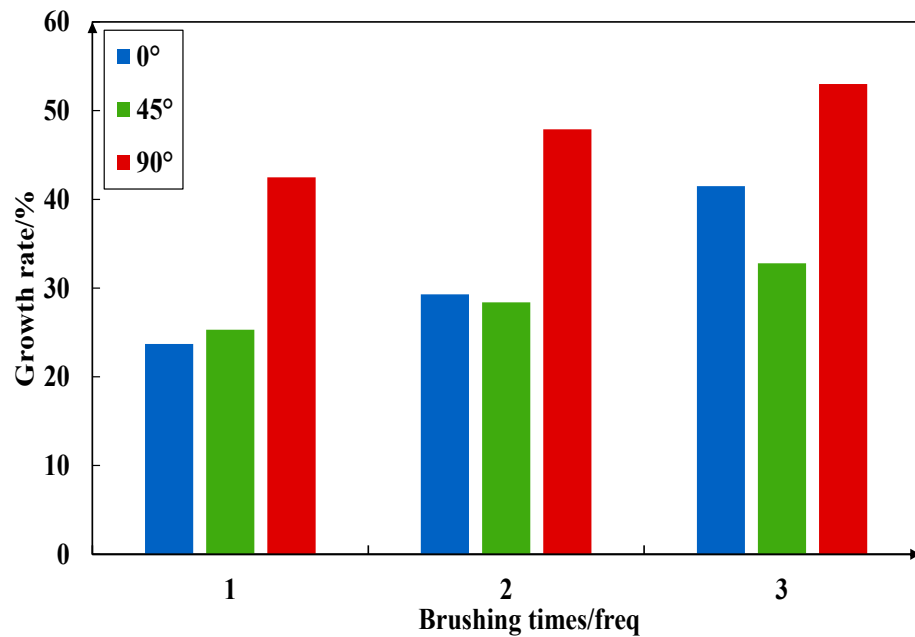**Figure 25.** Changes in flexural strength of specimens after repair by PTSL.

Figure 26. Rate of increase in flexural strength of specimens repaired by PTSL.

This paragraph analyzes the reasons for the above phenomenon. The extension of PTSL was 172 mm and the viscosity was 4200 MPa·s. The amount of its penetration into the pores of PR was less, which led to a smaller stress concentration area. Consequently, the main thing that determined the strength of PR-TSL was the degree of filling and repairing of the prefabricated cracks. The viscosity of PTSL was the largest among the three TSLs. When PR-TSL were subjected to compression, PTSL filled around the prefabricated cracks, providing good support and preventing the destruction of the prefabricated cracks. When PR-TSL were subjected to tension, the PTSL was well-bonded to both sides of the prefabricated cracks with its high viscosity [39,40]. PTSL relied on its high flexural strength to make itself more difficult to break and to stop the deformation of the cracks. Consequently, PTSL showed a good repair effect with a single brushing slurry. However,

with the increase in the number of brushing times, the growth of the repair effect slowed down, possibly indicating a saturation threshold of the repair effect.

3.3. Comparative Analysis of Three TSLs' Repair Performance

Among all the above trend lines, the three TSLs have the best fit to the repair trend lines of PR containing 90° crack, and their R^2 values are greater than 0.96. Therefore, the repair results of TSLs on PR containing 90° cracks were selected as representative. The repair performance of the three TSLs was compared and analyzed (Figure 27).
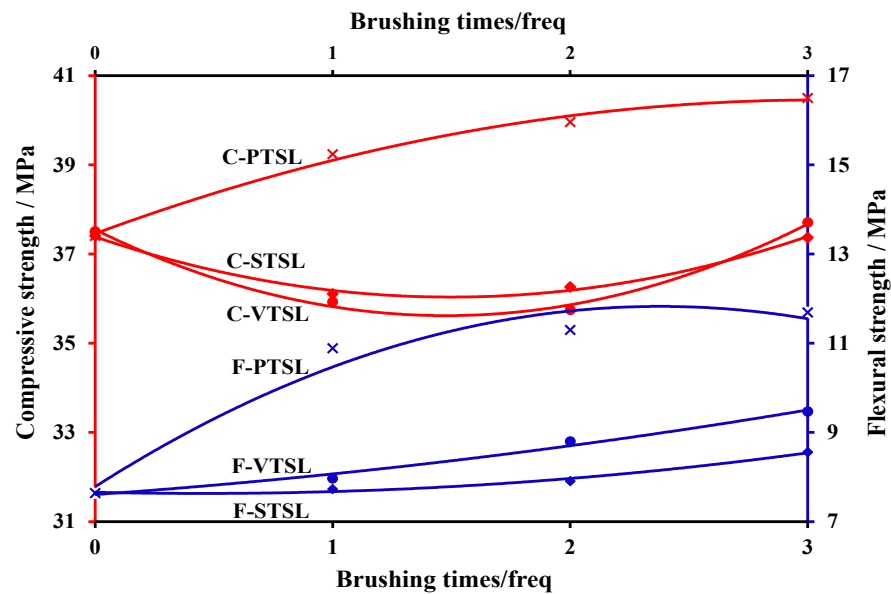
Figure 27. Changes in strength after repair of rock-like specimens with 90° cracks.

In Figure 27, C-STSL demonstrates the changes in compressive strength of PR after it was repaired by STSL. C-VTSL demonstrates the changes in compressive strength of PR after it was repaired by VTSL. C-PTSL demonstrates the changes in compressive strength of PR after it was repaired by PTSL. F-STSL demonstrates the changes in flexural strength of PR after it was repaired by STSL. F-VTSL demonstrates the changes in flexural strength of PR after it was repaired by VTSL. F-PTSL demonstrates the changes in flexural strength of PR after it was repaired by PTSL.

From Figure 27, it can be seen that PTSL was better than STSL and VTSL in repairing PR. The results of the compressive strength test showed that the repair effect of STSL on PR was similar to that of VTSL. However, the flexural strength test results showed that the repair effect of VTSL on PR was slightly better than that of STSL. Therefore, it was concluded that the repair performance of VTSL was slightly better than that of STSL in the experiment. Both trend lines, C-PTSL and F-PTSL, showed a tendency to increase in strength as the number of brushing times increased. There was a significant increase in strength when the PTSL was brushed once, which suggests that PTSL can be brushed once to achieve good repair. However, the increase in repair results was not significant with the increase in the number of brushing times. Therefore, PTSL was selected as the best restoration material.

According to the basic performance of PTSL in Table 5, PTSL has relatively good mechanical properties and viscosity, but the flowability of PTSL is relatively poor. The next step will be to conduct research on enhancing the fluidity of the PTSL.

3.4. Correlation Analysis between Different Crack Angles and PTSL Repair Performance

Figure 28 demonstrates that the unrepaired PR containing a 45° crack is the most easily damaged in the compressive experiments. The compressive strengths of PR containing

0° cracks and PR containing 90° cracks are close to each other. This is consistent with the previous study [41–43]. However, PR containing a 45° crack is not the most easily damaged when the slurry is brushed twice.
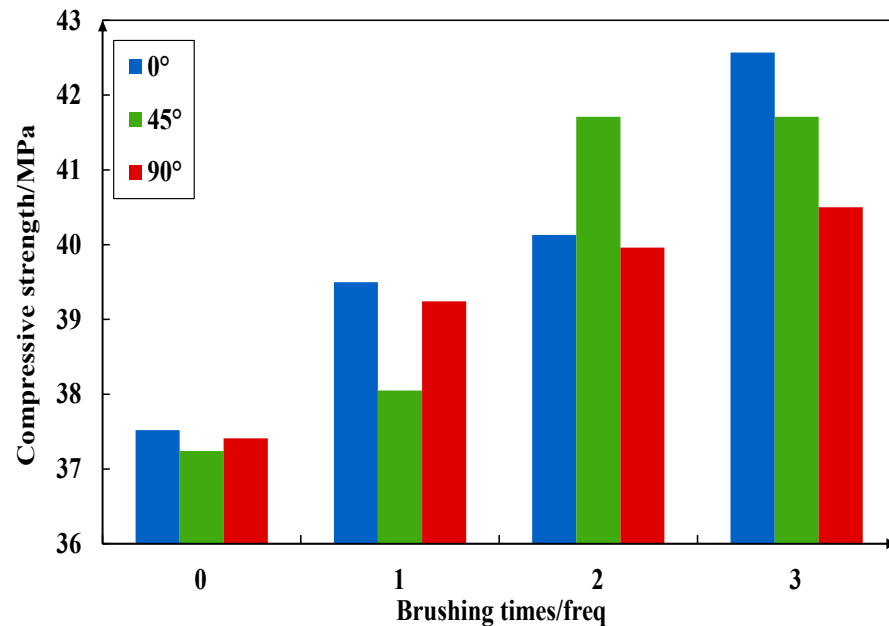

Figure 28. Changes in compressive strength of specimens after repair by PTSL.

Figure 29 demonstrates that the unrepaired PR containing a 90° crack is the easiest to damage in the flexural experiments, and the flexural strengths of PR containing 0° cracks and PR containing 45° cracks are significantly higher than that of PR containing a 90° crack. However, after repair by PTSL, the flexural strength of PR containing a 90° crack is significantly increased, and PR containing a 90° crack becomes the most difficult specimen to damage.
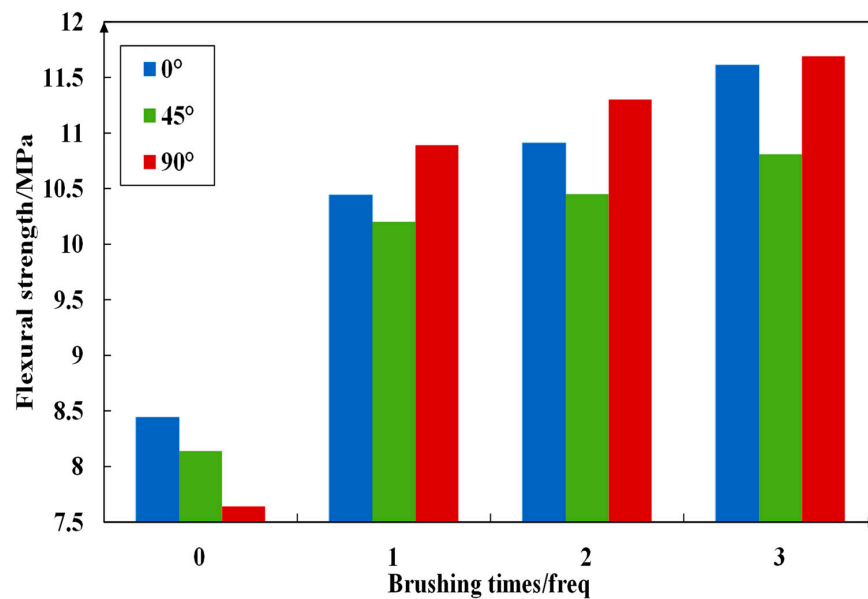

Figure 29. Changes in flexural strength of specimens after repair by PTSL.

In conclusion, the strength of PR is obviously improved after being repaired by PTSL. PTSL is effective in repairing low-strength PR and has excellent repair performance.

4. Conclusions

By studying the changes in compressive and flexural strength of PR-TSL, the main conclusions obtained are as follows:

(1) When the number of brushing times was 1 or 2, PR containing 0°, 45°, and 90° cracks were repaired by STSL and VTSL. The compressive and flexural strength of PR-TSL were found to decrease to different degrees. This may be due to the fact that the two TSLs existed within the cracks as monstrosities, which led to the stress concentration causing strength reduction. In contrast, PTSL was effective in repairing the three cracks. This was due to the fact that it connected the cracks with high viscosity and increased the resistance of the cracks to deformation.

(2) For the three TSLs, when their brushing times were more than 3 and the brushing thickness was greater than or equal to 4.2 mm, all three TSLs showed repair effects, but the PTSL had the best repair effect. This can be attributed to the fact that TSL completely filled the cracks and had a bonding effect on both ends of the cracks. The increase in strength caused by the bonding effect was greater than the decrease in strength caused by stress concentration; thus, they showed a repair effect.

(3) The repair effects of the three TSLs on PR were, in descending order, PTSL, VTSL, and STSL. PTSL is effective in repairing low-strength PR and has excellent repair performance. As the thickness of the brush slurry increased, its repair performance continued to improve.

References

1. Yang, X.; Yu, H.; Wang, Y.; Cheng, W. Investigation of dust pollution control rules in tunnel excavation based on modularized airflow diverging system. *Build. Environ.* **2022**, *221*, 109356. [CrossRef]
2. Yang, X.; Yu, H.; Zhao, J.; Cheng, W.; Xie, Y. Research on the coupling diffusion law of airflow-dust-gas under the modularized airflow diverging dust control technology. *Powder Technol.* **2022**, *407*, 117703. [CrossRef]
3. Lian, X.; Zhang, Y.; Liu, J.; Deng, W.; Guo, J.; Cai, Y. Rules of overburden crack development in coal mining with different ratios of rock-soil strata conditions. *Arab. J. Geosci.* **2022**, *15*, 511. [CrossRef]
4. Xu, J.; Pu, H.; Sha, Z. Full-Field Deformation and Crack Development Evolution of Red Sandstone under Impact and Chemical Erosion. *Minerals* **2022**, *12*, 1038. [CrossRef]
5. Wu, G.; Sun, M.; Song, K.; Zhai, M. Analysis of crack development or closure state of soil overlying thin bedrock based on water flow measurement experiment. *Arab. J. Geosci.* **2022**, *15*, 1327. [CrossRef]
6. Tripathi, R.; Hloch, S.; Chattopadhyaya, S.; Klichová, D.; Klich, J. Influence of frequency change during sandstone erosion by pulsed waterjet. *Mater. Manuf. Process.* **2020**, *35*, 187–194. [CrossRef]
7. Lv, W.; Sun, C.; Shen, B. Experimental study on damage evolution and crack propagation characteristics of sand stone under combined stress state. *J. Shandong Univ. Sci. Technol. (Nat. Sci. Ed.)* **2020**, *39*, 37–45.

8. Li, Y.; Yan, H.; Sun, S.; Zhang, L.; Zhang, S.; Li, Z. Experimental study on the expansion law and mechanical characteristics of crack propagation in rock with composite defect. *J. Shandong Univ. Sci. Technol. (Nat. Sci. Ed.)* **2022**, *41*, 42–50.

9. Liu, Q.; Wang, Q.; Wu, P.; Wu, J.; Lv, X. Research progress in application of red mud in cementitious materials. *J. Shandong Univ. Sci. Technol. (Nat. Sci. Ed.)* **2022**, *41*, 66–74.

10. Li, L.; Hagan, P.C.; Saydam, S.; Hebblewhite, B. Shear resistance contribution of support systems in double shear test. *Tunn. Undergr. Space Technol.* **2016**, *56*, 168–175. [CrossRef]

11. Guner, D.; Ozturk, H. Experimental and modelling study on nonlinear time-dependent behaviour of thin spray-on liner. *Tunn. Undergr. Space Technol.* **2019**, *84*, 306–316. [CrossRef]

12. Mpunzi, P.; Masethe, R.; Rizwan, M.; Stacey, T.R. Enhancement of the tensile strengths of rock and shotcrete by thin spray-on liners. *Tunn. Undergr. Space Technol.* **2015**, *49*, 369–375. [CrossRef]

13. Tannant, D.D. Thin Spray-on Liners for Underground Rock Support. In Proceedings of the 17th International Mining Congress and Exhibition of Turkey-IMCET 2001, Ankara, Turkey, 19–22 June 2001.

14. Li, Z.; Nocelli, B.; Saydam, S. Effect of rock strength and surface roughness on adhesion strength of thin spray-on liners. *Int. J. Rock Mech. Min. Sci.* **2017**, *91*, 195–202. [CrossRef]

15. Qiao, Q.Q.; Nemcik, J.; Porter, I.; Baafi, E.; Zhang, Z.Y.; Shan, Z.J. Development of Testing Methods of Thin Spray-on Liner Shear-Bond Strength. In Proceedings of the ISRM Regional Symposium—EUROCK 2014, Vigo, Spain, 27–29 May 2014.

16. Ozturk, H.; Tannant, D.D. Influence of rock properties and environmental conditions on thin spray-on liner adhesive bond. *Int. J. Rock Mech. Min. Sci.* **2011**, *48*, 1196–1198. [CrossRef]

17. Qiao, Q.; Nemcik, J.; Porter, I.; Baafi, E. Laboratory investigation of support mechanism of thin spray-on liner for pillar reinforcement. *Géotech. Lett.* **2014**, *4*, 317–321. [CrossRef]

18. Ozturk, H.; Tannant, D.D. Thin spray-on liner adhesive strength test method and effect of liner thickness on adhesion. *Int. J. Rock Mech. Min. Sci.* **2010**, *47*, 808–815. [CrossRef]

19. Chen, L.; Zhou, Z.; Liu, G.; Cui, X.; Dong, Q.; Cao, H. Effects of substrate materials and liner thickness on the adhesive strength of the novel thin spray-on liner. *Adv. Mech. Eng.* **2020**, *12*, 1687814020904574. [CrossRef]

20. Dong, Q.; Chen, L.; Cheng, W.; Liu, Z.; Cui, X.; Liu, G.; Shi, Z.; Sun, Z.; Zhang, Y. Material Performance Tests of the Polymer-Cement Thin Spray-On Liner. *Geofluids* **2020**, *2020*, 6647363. [CrossRef]

21. Chen, L.; Jiang, X.; Liu, Z.; Cui, X.; Liu, G.; Zhou, Z.; Dong, Q. Synthesis and Properties of a Polymer-Modified Material for Thin Spray-On Liners in Mine Roadways. *Adv. Mater. Sci. Eng.* **2020**, *2020*, 9789051. [CrossRef]

22. Huang, M.; Xiao, T. Mechanical and deformation properties of prefabricated monofissure-like rocks under uniaxial compression conditions. *J. Chang. Univ. (Nat. Sci. Ed.)* **2020**, *17*, 115–120.

23. Wu, W.; He, G.; Chen, K.; Xue, Y.; Wang, C.; Wang, Y. Breakage test and analysis of rock specimens with non-coplanar intermittent fissures. *Non-Ferr. Met. Eng.* **2021**, *11*, 107–116.

24. Liang, Q.; Cao, H. Mechanical characterization of single-fissure rocks under uniaxial compression. *China Water Transp. (Second Half Mon.)* **2021**, *21*, 151–153.

25. Xing, Y. Study on the Properties and Mechanism of Cementitious Composites Modified by Polyvinyl Alcohol. Ph.D. Thesis, Dalian University of Technology, Dalian, China, 2019.

26. Zhu, M. Preparation and performance study of Styrene-acrylic emulsion modified cement repair mortar. *Cem. Technol.* **2011**, *3*, 31–33.

27. Xie, Y.; Lin, X.; Li, H.; Ji, T. Effect of polyvinyl alcohol powder on the bonding mechanism of a new magnesium phosphate cement mortar. *Constr. Build. Mater.* **2020**, *239*, 117871. [CrossRef]

28. Mei, J.; Li, H.; Xu, Z. Effect of Styrene-Acrylic Emulsion on Crack Resistance of Cement-Based Materials. *Mater. Sci. Forum* **2021**, *1036*, 288–300. [CrossRef]

29. Cruz, E.O.; Radler, M.J.; Perello, M.; Savastano, H., Jr. Fiber cement boards modified with styrene-acrylic copolymer: An approach to address dimensional stability and cellulose fiber preservation. *J. Compos. Mater.* **2020**, *55*, 002199832095122. [CrossRef]

30. Bai, E.-L. Tensile properties of a flexible polymer-cement composite containing portland cement and vae emulsion. *Ceramics–Silikáty* **2019**, *64*, 1–9. [CrossRef]

31. Ohama, Y. Principle of Latex Modification and Some Typical Properties of Latex-Modified Mortars and Concretes Adhesion; Binders (materials); Bond (paste to aggregate); Carbonation; Chlorides; curing; diffusion. *Materials* **1987**, *84*, 511–518.

32. Beeldens, A.; Van Gemert, D.; Schorn, H.; Ohama, Y.; Czarnecki, L. From microstructure to macrostructure: An integrated model of structure formation in polymer-modified concrete. *Mater. Struct.* **2005**, *38*, 601–607. [CrossRef]

33. Cheng, J.; Shi, X.; Xu, L.; Zhang, P.; Zhu, Z.; Lu, S.; Yan, L. Investigation of the effects of styrene acrylate emulsion and vinyl acetate ethylene copolymer emulsion on the performance and microstructure of mortar. *J. Build. Eng.* **2023**, *75*, 106965. [CrossRef]

34. Shu, X.; Zhao, Y.; Liu, Z.; Zhao, C. A study on the mix proportion of fiber-polymer composite reinforced cement-based grouting material. *Constr. Build. Mater.* **2022**, *328*, 127025. [CrossRef]

35. Zhang, X.; Du, M.; Fang, H.; Shi, M.; Zhang, C.; Wang, F. Polymer-modified cement mortars: Their enhanced properties, applications, prospects, and challenges. *Constr. Build. Mater.* **2021**, *299*, 124290. [CrossRef]

36. Niu, Y.; Liu, G.; Zhong, Z.; Wang, J.; Zhang, R.; Liu, B. Numerical investigation on fracture characteristic and failure mechanism of rock-like materials with intermittent flaws under compressive-shear loading. *Constr. Build. Mater.* **2023**, *388*, 131698. [CrossRef]

37. Zheng, Z.; Tang, H.; Zhang, Q.; Pan, P.; Zhang, X.; Mei, G.; Liu, Z.; Wang, W. True triaxial test and PFC3D-GBM simulation study on mechanical properties and fracture evolution mechanisms of rock under high stresses. *Comput. Geotech.* **2023**, *154*, 105136. [CrossRef]

38. He, Z.; Xie, Z.; Zhang, N.; Han, C.; Xiang, Z.; Yan, G.; Qiao, H.; Shao, C. Research on spatiotemporal evolution law of surrounding rock fractures and hierarchical collaborative control technology in high-stress soft rock roadway: A case study. *Eng. Fail. Anal.* **2023**, *150*, 107366. [CrossRef]

39. Liu, F.; Wang, B.; Xing, Y.; Zhang, K.; Jiang, W. Effect of Polyvinyl Alcohol on the Rheological Properties of Cement Mortar. *Molecules* **2020**, *25*, 754. [CrossRef]

40. Bian, Y.; Huang, Y.; Li, F.; Dong, D.; Zhao, H.; Zhao, P.; Lu, L. Polyvinyl-Alcohol-Modified Calcium Sulphoaluminate Cement Repair Mortar: Hydration and Properties. *Materials* **2021**, *14*, 7834. [CrossRef] [PubMed]

41. Lee, H.; Jeon, S. An experimental and numerical study of fracture coalescence in pre-cracked specimens under uniaxial compression. *Int. J. Solids Struct.* **2011**, *48*, 979–999. [CrossRef]

42. Wang, Y.; Tang, J.; Dai, Z.; Yi, T. Experimental study on mechanical properties and failure modes of low-strength rock samples containing different fissures under uniaxial compression. *Eng. Fract. Mech.* **2018**, *197*, 1–20. [CrossRef]

43. Wong, L.N.Y.; Einstein, H.H. Systematic evaluation of cracking behavior in specimens containing single flaws under uniaxial compression. *Int. J. Rock Mech. Min. Sci.* **2009**, *46*, 239–249. [CrossRef]